Modified volcanic domes and associated debris aprons on Venus

M. H. BULMER[1] & J. E. GUEST

University of London Observatory, University College London, 33/35 Daws Lane, Mill Hill, London NW7 4SD, UK

[1] *Present address: Centre for Earth and Planetary Studies, National Air and Space Museum, Smithsonian Institution, Washington DC L0560, USA*

Abstract: The Magellan SAR images show that volcanic domes occur on the surface of Venus. Edifices with scalloped margins are similar to volcanic domes and fall within a spectrum ranging from unmodified to remnant forms. Over 320 domes have been located of which more than 80% have modified morphologies. Broadly, the modified domes can be described by five sub-categories which are related to three unmodified dome sub-categories. Many modified domes have deposits associated with them that possess characteristics indicative of their having been formed from mass movements. Evidence for slope failure is not seen on volcanic shields on Venus due to them having shallow flanks. Several steep-sided cones show some evidence of slope failure but on a much smaller scale than failures associated with domes. Slope failures on venusian domes appear to have been triggered by non-explosive and explosive events. Collapse on the edges of domes, either as a result of explosive events of oversteepening, is common on Earth but the collapses on Venus are on a scale that is more in common with major sector collapses of volcanoes on Earth. Four morphological sub-groups of debris deposit have been recognized. The deposits in groups one and two are analogous to terrestrial volcanic debris avalanche deposits and the deposits in group three are analogous to pyroclastic flows on Earth. The characteristics of the fourth group of deposits are similar to those resulting from deep-seated slides on Earth.

During the early stages of the Magellan mission a volcanic edifice with scalloped margins whose origin was enigmatic was found to the north of Alpha Regio (18.1°S, 5.5°E). As the mission progressed, other edifices with scalloped margins were identified. The radar characteristics and morphologies of many of these edifices are similar to volcanic domes and form a spectrum ranging from unmodified to remnant forms. Based on the characteristic margins, the edifices were termed scalloped margin domes, or SMDs (Guest *et al.* 1992*a*, *b*). Many of the domes are an order of magnitude larger than terrestrial domes. Debris aprons associated with modified domes possess a range of radar and morphologic characteristics indicative of mass movement deposits (Guest *et al.* 1991, 1992*a*, *b*; Bulmer *et al.* 1992, 1993). Large arcuate backscarps on the flanks of some domes indicate that large-scale collapses have occurred. There is an absence of debris aprons around some domes, which may be explained in some cases by burial by younger material. Elsewhere the deposits may form only a thin unconsolidated mantle that was penetrated by the radar or have the same radar backscatter as the surrounding plains.

Using the Magellan dataset an extensive database was compiled from a global survey of volcanic domes on Venus (Bulmer 1994). It incorporates information on the morphological and morphometrical aspects of domes and large debris aprons associated with them. Over 300 modified domes were identified during the survey indicating that if SMDs are modified volcanic domes, then domes are more common than suggested in previous work (Head *et al.* 1992; Pavri *et al.* 1992). A greater number of modified domes were identified than unmodified domes.

A range of morphological characteristics of modified domes was recognized from the survey but they can broadly be divided into five categories labelled MD1 to MD5. It is proposed that modified domes are derived from the different dome sub-categories D_1 to D_2 discussed in Guest *et al.* (1992*a*). As part of the global survey of modified domes, details of debris aprons associated with volcanic domes were compiled. Over 100 debris aprons were identified. The database includes information on the morphological and morphometric aspects of mass movement deposits. A descriptive classification using the headscarp–debris apron relationship, the surface texture and the plan view, was devised that allowed the deposits to be placed into one of four categories, labelled G1 to G4. These four different morphological groups exhibit distinctive radar characteristics and morphometrical trends. The data obtained from the survey were designed to build upon an extensive database of large landslides on

From McGuire, W. J., Jones, A. P. & Neuberg, J. (eds) 1996, *Volcano Instability on the Earth and Other Planets*, Geological Society Special Publication No. 110, pp. 349–371.

Table 1. *Morphological and morphometric characteristics of unmodified (D) and modified domes (MD)*

Type	Plan view	Profile	Diameter (km)	Height (m)	Slope (°)	Crater	Radar characteristics
D_1	Circular	Steep convex margins, relatively flat top	2–5	?	?	?	Radar-bright backscatter on foreslope
D_2	Circular	Steep convex slopes, raised rim	10	311	15	Single, central	Radar-bright backscatter, steep margins, steep rampart
D_3	Circular	Steep convex margins, rounded top	20–30	618	20	Single, often central	Radar-bright backscatter, steep margins
D_4	Near circular	Steep perimeter, concave inner surface	20	?	?	Surface downsagged	Radar-bright backscatter, steep margins. constant backscatter, inner surface
MD1	Circular	Steep slopes, conical	15–28	1500	27.4	Single, central	Radar-bright backscatter, steep slopes, often show lay-over
MD2	Circular	Steep sided with breaks of slope, convex summit area	17–32	1700	27.1	Single, central	Radar-bright backscatter, steep slopes, often show lay-over
MD3	Near circular	Flat upper surface, steep flanks	13–48	1200	28.2	Small pits	Radar-bright backscatter, steep slopes, often show lay-over on foreslopes
MD4	Circular	Steep sided, flat upper surface	23–50	1500	22.4	No pit craters identified	Radar-bright backscatter, steep slopes, often show lay-over
MD5	Circular	Steep slopes, concave inner surface	13–57	800	26.2	Large central downsag	Radar-bright backscatter, steep margins

Mars, the Moon and the Earth compiled by Shaller (1991), incorporating information on morphologic and morphometric aspects of large landslide phenomena.

Morphological characteristics of modified domes

When domes that have undergone only limited modification on the flanks are compared with the four dome categories D_1–D_4 (Guest *et al.* 1992*a*) morphological similarities are evident (Table 1). A sequence of progressively modified domes can be constructed that encompasses the different morphologies seen in the images. Domes have a range of planimetric forms, from those that have not been modified, to those that are nearly circular with small scallops, through to those that have irregular forms with little of the original edifice remaining. The majority of domes that are modified are greater than 10 km in diameter. The five sub-categories of modified domes represent only three categories of unmodified domes (Fig. 1).

The first group of modified domes (MD1) have steep flanks that rise to large central craters 5 km in diameter (Fig. 1). Some crater walls show evidence of slope failure and several of the edifices have flanks with distinct backscarps which are associated with debris aprons. Diffuse radar backscatter materials around the base of the majority of domes in this group are interpreted to be talus. Examples of domes in this group include a dome in Helen Planitia (31.7°S 260.2°E), that has steep flanks rising to a near-circular central crater. The northern flank of the dome has radial protuberances producing a stellate plan-form (Fig. 2). The central crater of another dome with the characteristics of this group situated in Ut Rupes (64.4°N, 306.6°E), is cross-cut by fractures which may have formed as a result of slope failure forming several small terraces (Fig. 3).

Modified domes in group two (MD2) are near-circular in plan-form, have gently convex upper surfaces and steep flanks with multiple breaks of slope (Fig. 1). The breaks in slope may have resulted from different eruptive pulses or phases. Several domes in this group have small summit craters a few kilometres in diameter. Diffuse radar backscatter materials interpreted to be talus are also observed around the base of the domes. Examples of domes in this group include a dome to the south of Atla Regio (16.2°S, 211.8°E) which has several breaks in

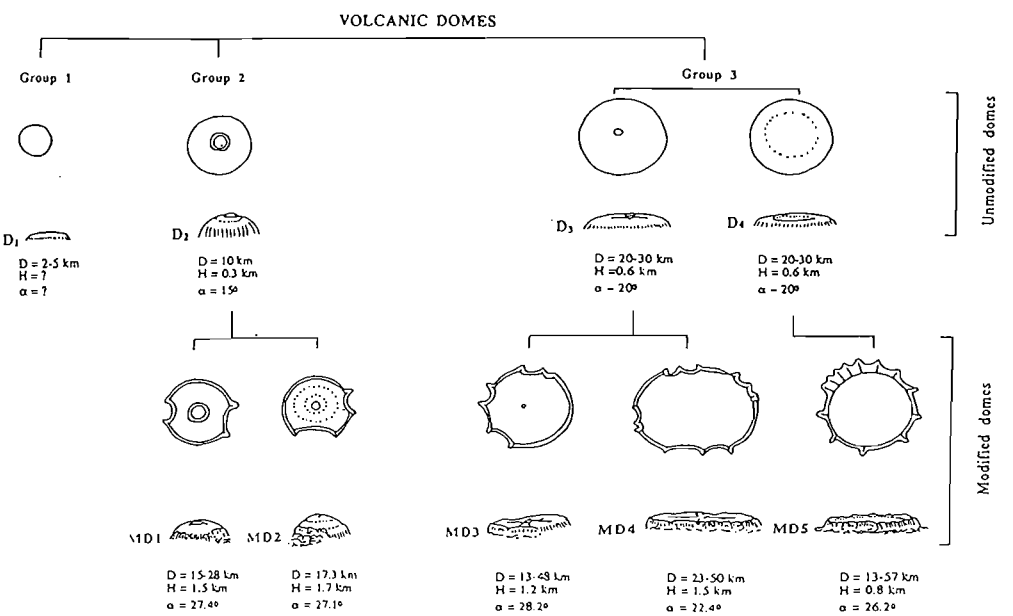

Fig. 1. Diagram showing a schematic representation of the modification of volcanic domes. In group 1 no modified forms related to D_1 were identified. In group 2 modified dome MD1 and MD2 are related to the unmodified dome sub-category D_2. In the third group of modified domes, MD3 and MD4 are related to unmodified domes in sub-category D_3. The modified dome MD5 is related to the unmodified sub-category D_4.

Fig. 2. Dome (md244) situated in Helen Planitia (31°S, 260.2°E). The dome has a diameter of *c.* 15 km and the characteristics of sub-category MD1. The upper surface of the dome is cross-cut by north to south trending fractures that do not extend into the surrounding plains. This indicates that the fractures were buried by younger lavas which may also have buried any debris aprons. The dome is situated in the floor of a volcano-tectonic structure. Magellan image C1 MIDR 30S261;1. Radar illumination is from the left.

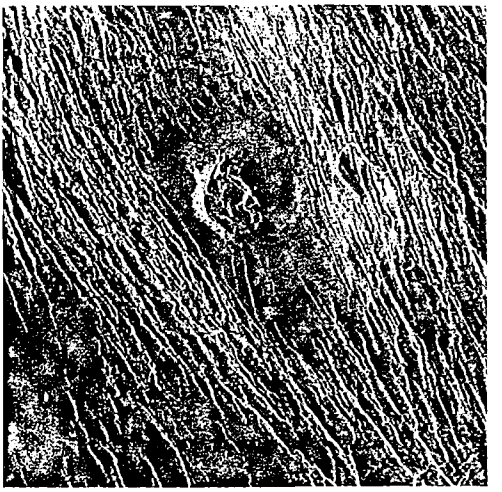

Fig. 3. Dome (md14) situated in Ut Rupes (64.4°N, 306.5°E). The dome is *c.* 15 km in diameter, is coded as i,a,2 and has the characteristics of sub-category MD1. The central crater has several terraces which may have formed from slope failure. The dome is superimposed on lavas that embay a northwest to southeast trending fracture set. Fractures trending north to south cross-cut the dome indicating they are younger than the dome. Magellan image C1 MIDR 60N319;1. Radar illumination is from the left.

slope (Fig. 4). The southern flank of the dome has several distinct backscarps that extend from the lower slopes to the summit.

The third group of modified domes (MD3) have slope angles of approximately 30° that rise to a flat upper surface (Fig. 1). Small central depressions and pits are common on the upper surfaces. The central depressions are likely to be the result of magma withdrawal at the end of the eruptive episode. The pits may have formed as a result of minor explosive events. Examples of the range of morphologies possessed by domes in this group include a little-modified dome situated in Tinatin Planitia (12.1°N, 8.9°E). Numerous small pit craters are present on the upper surface of the dome, but the margins are largely unmodified (Fig. 5). A more degraded dome to the north of Mokosha Mons (61.5°N, 248°E) has radial protuberances on the flanks and numerous small pit craters as well as fractures on the upper surface (Fig. 6). An example of a remnant dome occurs to the west of Phoebe Regio (7.6°S, 256°E). Little of the original dome remains and debris aprons occur at the base of individual scallops (Fig. 7).

Modified domes in group four (MD4) typically have near-circular or elongated plan-forms and have large diameter to height ratios with steep flanks (>20 km) that rise to extensive flat upper surfaces (Fig. 1). Several of these large-volume domes have downsags. An example of one such downsagged dome (Fig. 8), is situated on the summit region of a shield volcano in Navka Planitia (8.8°S, 305.3°E). Domes with the characteristics of this group that are situated on ridge-belts are often heavily modified, such as one in Bereghinya Planitia (48.9°N, 16°E). The dome is heavily modified by younger cross-cutting fractures (Fig. 9).

Modified domes in the fifth group (MD5), have concave upper surfaces with relatively uniform radar backscatter cross-sections (Fig. 1). The downsagged surfaces on several of the domes in the group are bounded by complex sets of terraces possibly resulting from several stages of caldera collapse. Radar-dark backscatter materials seen on the floor of some calderas may be congealed lavas. The majority of the domes in this group have near-circular plan-forms with stellate perimeters produced by coalesced backscarps. Some of the backscarps have radar-bright talus slopes at their bases and extensive mass movement deposits associated with them. One of the best examples of this

Fig. 4. A dome (md176), situated in plains to the south of Atla Regio (16.2°S, 211.7°E). The gently convex upper surface and steep slopes are characteristic of dome sub-category MD2. The dome has a diameter of 26 km, and an average slope angle of 24.3° and a calculated height of 2.8 km. The south flank has undergone a number of mass movements. The debris aprons are younger than the plains since the fractures do not cross-cut them. Magellan image C1 MIDR 15S215;1. Radar illumination is from the left.

dome morphology is situated on the northern margin of Alpha Regio (18.1°S, 5.5°E). The dome has a distinctive stellate plan-form with numerous radial protuberances and a concave interior which may have formed as a result of a breach to the west (Fig. 10).

Morphometrical characteristics of modified domes

The diameters of modified domes range from <10 km to 120 km with the majority ranging between 10 km and 35 km (Fig. 11). Domes with diameters greater than 70 km tend to consist of several superimposed or coalesced domes whose margins are often indistinguishable (4°N, 19°E). Over 300 modified domes are identified on the surface of Venus compared with a total of 154 domes found in a previous study (Pavri *et al.* 1992). The reason for the difference in numbers is, we believe, that a spectrum exists from unmodified to highly modified domes. This allowed remnant volcanic edifices to be examined and their likely original forms determined.

Only a limited number of dome heights were obtained from the altimetry data owing to the resolution of the data. The majority of heights were calculated using the symmetry of the volcano seen in the SAR images. The calculated heights of modified domes range from 0.4 km to 3.8 km (Fig. 12). The mean height is 1.3 km which is four times the mean for terrestrial sub-aerial domes. However, the mean height values can be used only as a guide since the calculation of height using radar clinometry required domes to have near-circular plan-forms and includes inaccuracies in measurements from the digital data of ±150 m. This criterion prevented the heights of many modified domes from being obtained. The tendency for domes on Venus to be larger than on Earth is confirmed by a plot of the relationship between height and diameter (Fig. 13). Domes on Venus are, in many instances, an order of magnitude larger in diameter than terrestrial sub-aerial domes. The altitudinal range in the distribution of domes is from 1.4 km below datum to 2.9 km above datum. The majority are located between 6051.0 km and 6052.0 km mean planetary radius, very close to the mean planetary radius of 6051.8 km.

Morphological characteristics of debris deposits associated with modified domes

Four different morphological groups of debris aprons can be recognized from the 105 debris aprons identified from the global survey (Bulmer 1994). Each groups has distinctive radar characteristics and morphometric trends. Deposits in the first group (G1) cover large areas (>100 km^2), have long travel distances (>20 km) and are characterized by hummocky topography. The surface textures of the deposits are rough on a coarse scale, consisting of large hummocks (>1 km), surrounded by a matrix of material. In plan view, the deposits are often fan-shaped or lobate. Some large debris aprons extend from the base of a dome, while other deposits are discontinuous with the base, lying beyond the margins of a dome.

An example of deposits in group one (G1) is in Helen Planitia (at 29.5°S, 183.6°E). It consists of massive hummocks and has fan-shaped plan form with well-defined lobate margins (Fig. 14). The deposit is discontinuous with the base of the dome. Another dome, in eastern Mokosha Mons (55°N, 266°E) has a large sector detached on the east flank (Fig. 15). The large hummocks at the base of the dome and the extensive deposits that extend outwards across plains, may have formed from the failed sector having

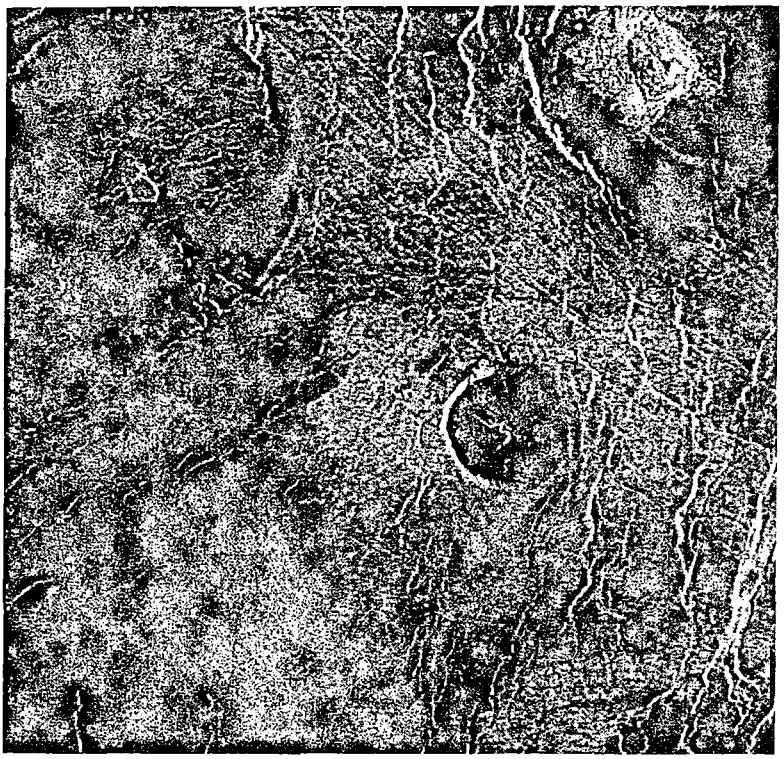

Fig. 5. A dome (md111) situated in Tinatin Planitia (12.1°N, 8.9°E). The dome is *c.* 20 km in diameter and has the characteristics of sub-category MD3. The dome has undergone little modification but numerous small pits occur on the upper surface. The dome is situated on the margin of concentric fractures that define a volcano-tectonic structure. Magellan image C1 MIDR 15N009;1. Radar illumination is from the left.

moved initially as a coherent mass before it collapsed catastrophically. It seems likely that the failure occurred after the eruption had ceased and the dome had become solid. This then explains the massive nature of the deposits and why the mass initially underwent only limited disintegration during motion. A dome in Guinevere Planitia (14°N, 229°E) has a large detached debris apron made up of large hummocks which form the margin of the fan-shaped deposit (Fig. 16). The origin of the debris is enigmatic. The absence of debris towards the base of the dome may be explained if the collapsed mass moved away from the dome as a coherent mass prior to disintegrating. If the debris apron formed as a result of one massive failure, a clear debris–headscarp relationship would be expected. However, no such relationship is observed. One possibility is that the failure occurred on a previous dome which was de-stroyed, and that a new dome has been emplaced subsequently. Alternatively, after the initial massive failure, subsequent smaller volume slope failures, that formed the small embayments on the west flank, may have buried large hummocks close to the base of the dome.

Only a few examples of deposits in the second group (G2) have been identified. The debris aprons are often detached from the base of the dome and have narrow proximal zones that spread laterally towards the distal zone. The deposits have a lower radar backscatter coefficient than the deposits in group one, owing to smoother surface textures made up of smaller dispersed radar-bright hummocks ($\leq$1 km). In plan view, the deposits have irregular lateral and distal margins.

One dome in Navka Planitia (26°S, 296.7°S) has at least five debris aprons with the characteristics of subcategory G2 (Fig. 17). The proximal zones of the debris aprons are situated some distance from the base of the slopes from where they originated. The aprons of debris are made up of dispersed radar-bright hummocks. The long and narrow plan-forms of the deposits are characteristic of debris masses

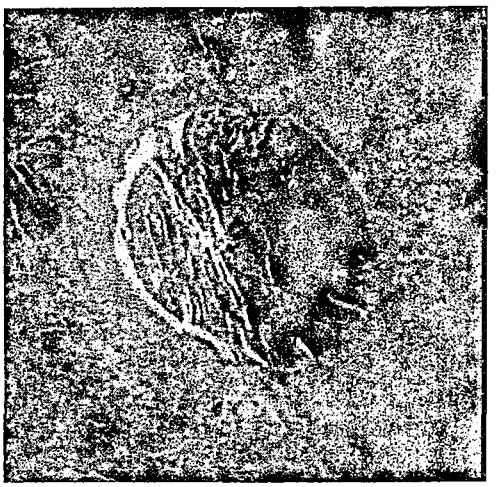

Fig. 6. A dome (md17) situated north of Mokosha Mons (61.5°N, 248°E), with the characteristics of subcategory MD3. The dome has a 50 km diameter and an average slope angle of 24°. The calculated height of the dome is 5.8 km. The radar-bright lavas that surround the dome appear to mantle the underlying fractured plains. The fractures on the dome can no longer be traced on the plains as they have been buried by subsequent lavas indicating the dome is an old feature.These younger lavas may have buried any debris aprons. Magellan image C1 MIDR 60N236;1. Radar illumination is from the left.

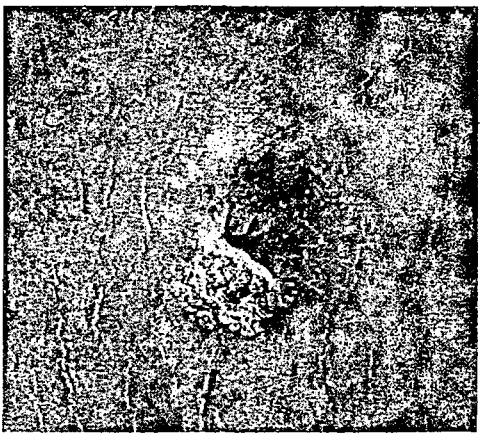

Fig. 7. Dome (md159) situated west of Phoebe Regio (7.6°S, 256°E). The diameter of the remnant dome is *c.* 25 km and the calculated height is 1.6 km. The dome has the characteristics of sub-category MD3. The margin of the dome is heavily scalloped and debris aprons occur around the base. Only a small part of the horizontal upper surface remains due to the central crater having undergone several stages of collapse. The debris aprons mantle the surrounding fractured plains. Magellan image
C1 MIDR 00N249. Radar illumination is from the left.

that travelled away from the dome at relatively high velocity, thereby influencing their form and accounting for location of the proximal zones. The presence of large hummocks in the deposits indicates that the source was solid and the debris mass underwent only limited disintegration during runout. The lack of well-defined boundaries around the deposits and the lower radar backscatter coefficient than deposits in group one may also reflect the influence of post-deposition reworking processes. For example, younger material may have mantled deposits partly burying them. In addition, chemical and physical erosion could have subdued the surface textures causing lower backscatter coefficients by reducing roughness.

The deposits in group three (G3) tend to be narrow and typically have debris aprons attached to the lower slopes of domes. They have shorter runout distances ($\leq$20 km) than deposits in groups one and two. Some of the deposits can be traced up into embayments or to backscarps. The debris aprons spread laterally once they were no longer confined to the troughs down which they travelled. Often the material embays the local topography surrounding a dome. The uniform radar-dark backscatter of the material indicates that the surficial textures are relatively smooth composed of small fragments >4 mm. In plan view the deposits have irregular lateral and distal margins.

Two domes on the summit of the shield volcano Sapas Mons (8.5°N, 188.2°E), have deposits with the characteristics of group three (Fig. 18). Radar-dark deposits around these domes can be traced back up into the heads of scallops suggesting they originated near the top of dome margins. The collapsed materials appear to have been confined as they descended down existing troughs on the flanks of the domes, spreading out once they reached the base of the slope. Some of the deposits were controlled by, and now embay, local topography.

Large failures with broad steep scarps characterize deposits in the fourth group (G4). They are the most common category of deposits. The deposits have travel distances <20 km and

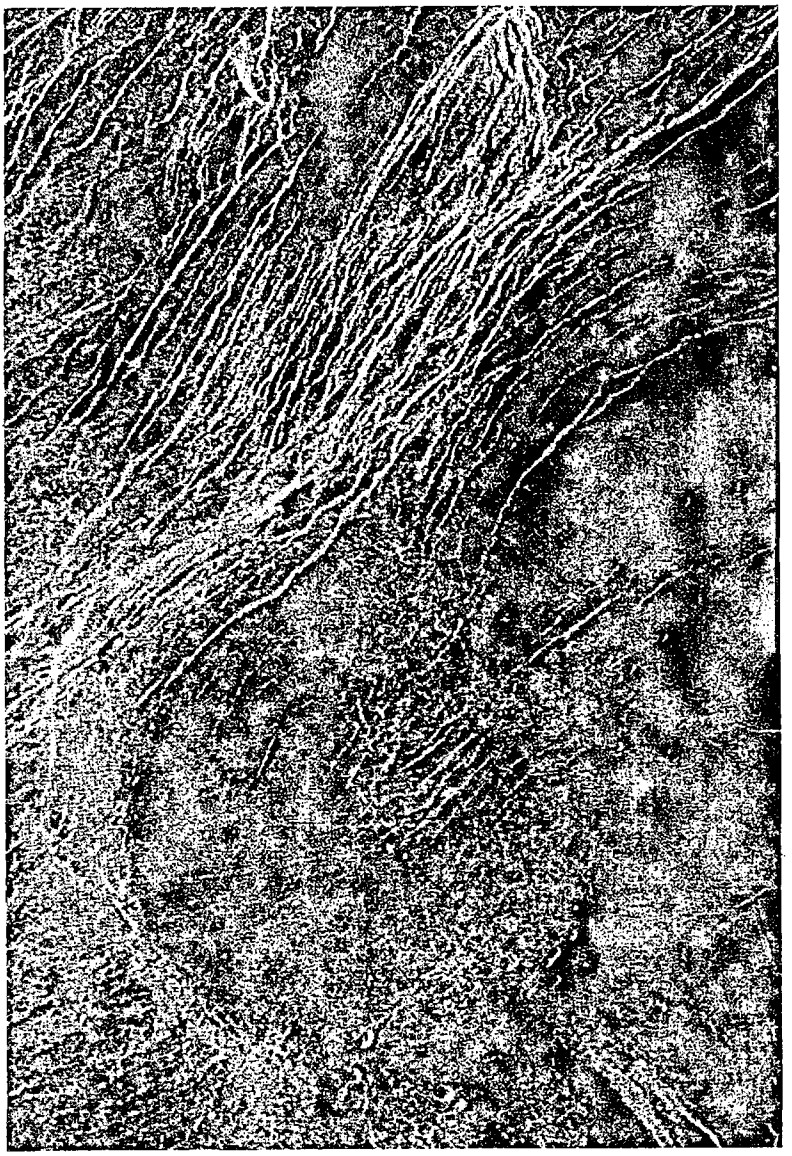

Fig. 8. Dome (md90) situated north of Atla Regio (18°N, 195.9°E). The dome diameter is *c.* 60 km. The dome has the characteristics of sub-category MD4. The concave upper surface may have resulted from magma withdrawl or degassing. Pit craters can be seen on the southern margin. The dome is superimposed on lavas associated with a volcanic centre to the south. The NE–SW trending fractures are younger than the dome since they cross-cut the upper surface and may have been influenced by the downsag. Magellan image C1 MIDR 15N197;1. Radar illumination is from the left.

the proximal zone is at the foot of the slope from which they originated. The surface textures of the deposits in this group appear to be related to the size of failure and distance they travelled. Large blocks tend to have relatively smooth gross textures, whereas disintegrated debris has a rough gross texture. In plan-form the deposits are either blunt with near-parallel lateral and distal margins, or lobate with convex lateral and distal margins.

Domes with the characteristics of group four such as one in Niobe Planitia (27.5°N, 134.8°E)

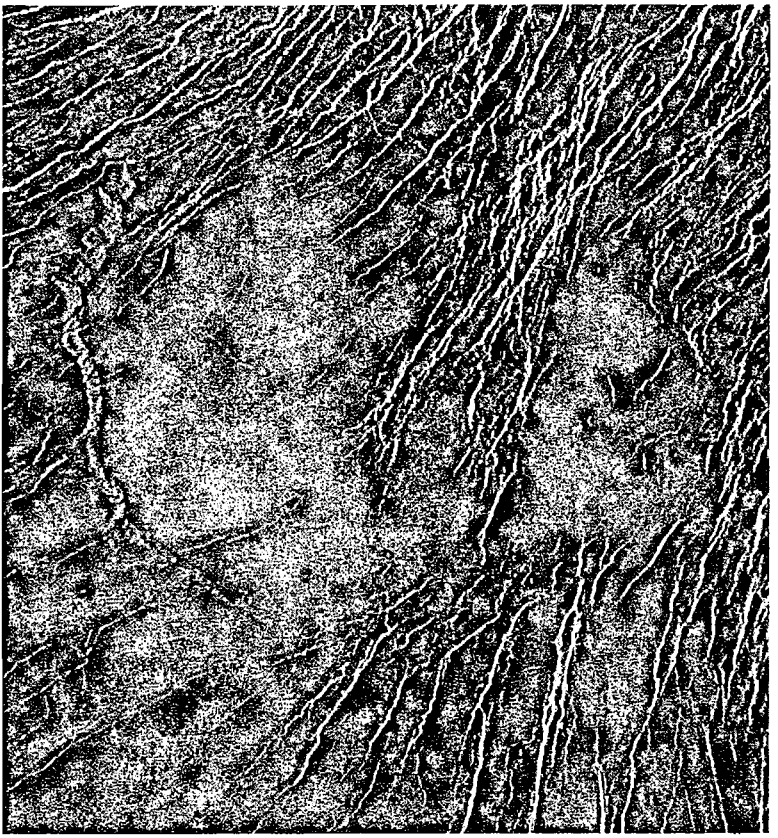

Fig. 9. An example of a dome (md29) in sub-category MD4, situated in Bereghinya Planitia (48.9°N, 16°E). The dome has a diameter of 50 km. The fractures trending northeast to southwest are younger than the dome. Magellan image C1 MIDR 45N011;1. Radar illumination is from the left.

have a large sector collapse (Fig. 19). The failed sector has remained largely intact and shows no evidence of back-tilting suggestive of a rotational component, indicating that the failure was planar. The lack of break-up of the failed sector may be explained, in part, by the short travel distance of the mass. The failure of the dome margin appears to have occurred after the eruptive activity had ceased and the dome had become rigid. Another dome in Navka Planitia (25.4°S, 308°E) has two deposits composed of large blocks that travelled away from the base of the dome (Fig. 20). One debris apron travelled to the northwest and the other moved to the northeast. The collapse to the northwest removed a large sector of the dome slope leaving a steep backscarp. The nature of the backscarp suggests that the slope failure was deep-seated. The large steep-sided block forming the proximal portion of the slide indicates that part of the slide remained coherent and may have moved with a rotational component. The distal zone shows a well-defined steep lobate margin. This may be explained if the failed rock mass underwent little disintegration and came to rest as several large blocks. If the failure was essentially rotational, the distal region would formerly have been the base of the dome slope that may have undergone severe distortion and fracturing. Once the base failed, the upper part of the slope would have pushed the collapsed material outwards as it back-tilted during rotation. The deposit to the northeast of the dome appears to have been shallower than the one to the northwest and the deposits are less coherent containing smaller blocks. Both failures are thought to have occurred after the eruption had ceased and the dome had become rigid.

Another dome to the south of Atla Regio (16.2°S, 211.7°E), has a series of well-defined arcuate backscarps that may have formed as a

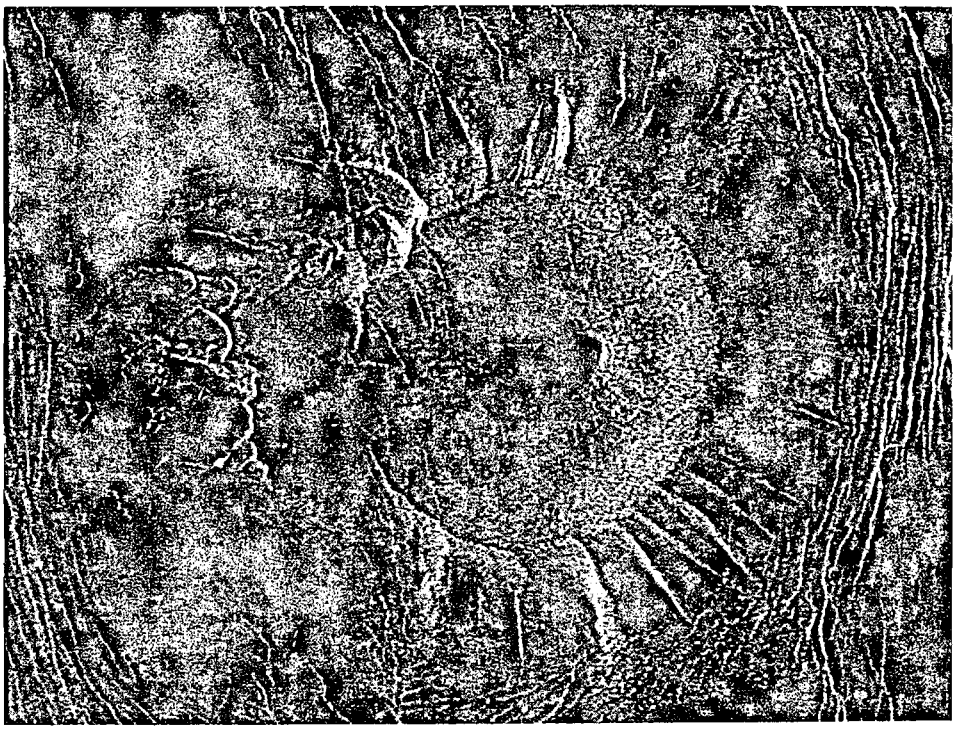

Fig. 10. An example of a dome (md184) in sub-category MD5, situated on the northern margin of Alpha Regio (18.1°S, 5.5°E). The dome has a diameter of *c.* 50 km, an average slope angle of 26.2° and a calculated height of 1 km. A central crater is visible and it appears the dome was breached on the west flank. Magellan image C1 MIDR 15S009;1. Radar illumination is from the left.

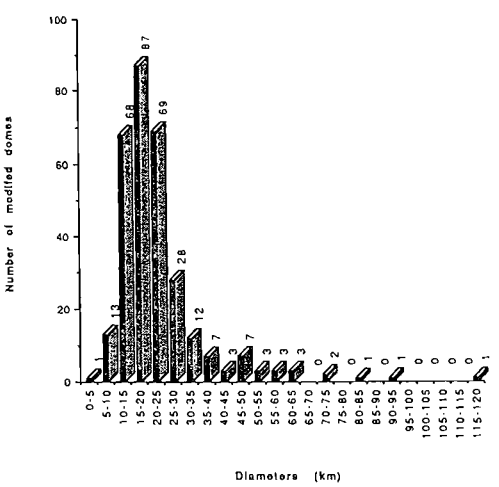

Fig. 11. Histogram showing the range of diameters of modified domes from a global population of 306.

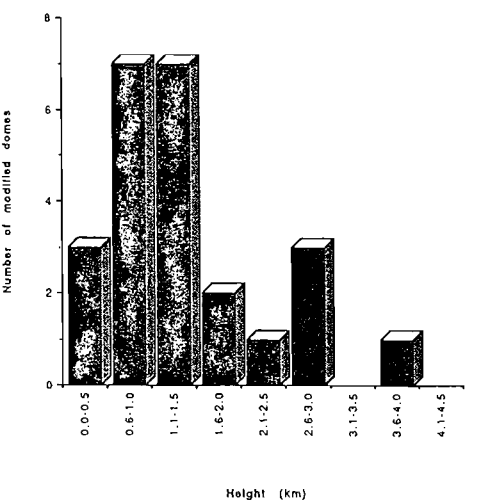

Fig. 12. Histogram showing the height of modified domes from a global population of 24.

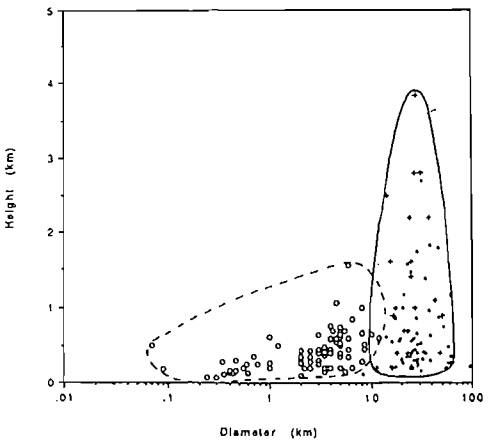

Fig. 13. Diagram showing the trend of domes on Earth and domes on Venus plotted as height vs. diameter. The open circles (○) show data for terrestrial sub-aerial domes, the dots (●) show data for unmodified domes on Venus (from Pavri *et al.* 1992), and the crosses (+) show data for modified domes on Venus.

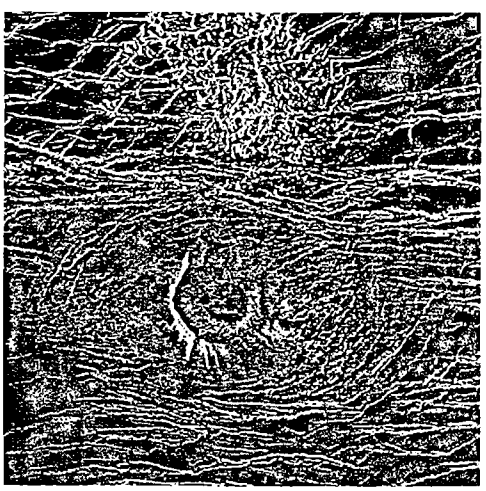

Fig. 14. A dome (md223) with the morphological characteristics of sub-category MD5, situated in Helen Planitia (29°S, 183.6°E). The dome has a diameter of *c.* 15 km and a height of 0.9 km. The debris apron has characteristics of group one (G1). The debris apron extends *c.* 40 km, contains large blocks and has a lobate plan-form. The proximal zone is detached from the dome's lower slopes. Fractures trending east to west cross-cut the debris apron. Magellan image C1 MIDR 30S189;1. Radar illumination is from the left.

series of slides during a single phase. Alternatively, successive slope failures may have occurred after an initial slide had destabilized the slope (Fig. 21). The failures are deep-seated and a large section of the dome has collapsed. In spite of the size of slope failures, deposits travelled only short distances. This can be explained by the slope breaking into large coherent blocks which then moved as a series of failures, each on a curved surface.

Morphometric characteristics of debris deposits

Twenty domes in the global survey have more than one associated deposit, but the majority have only one large debris deposit (Fig. 22). Despite many of the larger debris aprons being detached from the base of the dome, the travel distance of a deposit was measured in this survey from the toe of the debris mass to the base of the dome. It was not measured from the toe to the uppermost point of the headscarp because of problems in distinguishing headscarps on many slopes, due to distortions in the images. The horizontal lengths travelled by the debris range from 2.1 km to 81.6 km, with a mean length of 22.7 km. The majority of debris travelled <10 km from the base of the dome (Fig. 23). Within the different morphological groups, those in the first (G1) have travel distances that range between *c.* 20 km and *c.* 80 km with a mean of *c.* 40 km (Table 2). The lengths of deposits in the second group (G2) are similar to those in group one and range between *c.* 15 km and *c.* 70 km with a mean of *c.* 45 km. Deposits in group three (G3) have smaller run-out lengths ranging between *c.* 10 km and *c.* 20 km with a mean of *c.* 15 km. The distances travelled by deposits in group four (G4) range between *c.* 0 km and *c.* 20 km with a mean of *c.* 10 km.

For all the debris deposits associated with domes, the horizontal distance across the widest section of the deposits, ranges from 0.5 km to 62.5 km with a mean of 17.2 km (Fig. 24). The deposits in group one have the greatest widths ranging between 4.2 km and 62.5 km with a mean of *c.* 30 km (Table 2). The widths of deposits in group two range between 6.8 km and 26.1 km with a mean of *c.* 15 km. Deposits in group three have smaller widths that range from 2.1 km to 12.8 km with a mean of *c.* 3 km. The widths of deposits in group four are greater than in group three, ranging from 0.5 km to 26.7 km.

The area covered by a debris apron was calculated by mapping a boundary around the toe of a deposit to the top of the headscarp

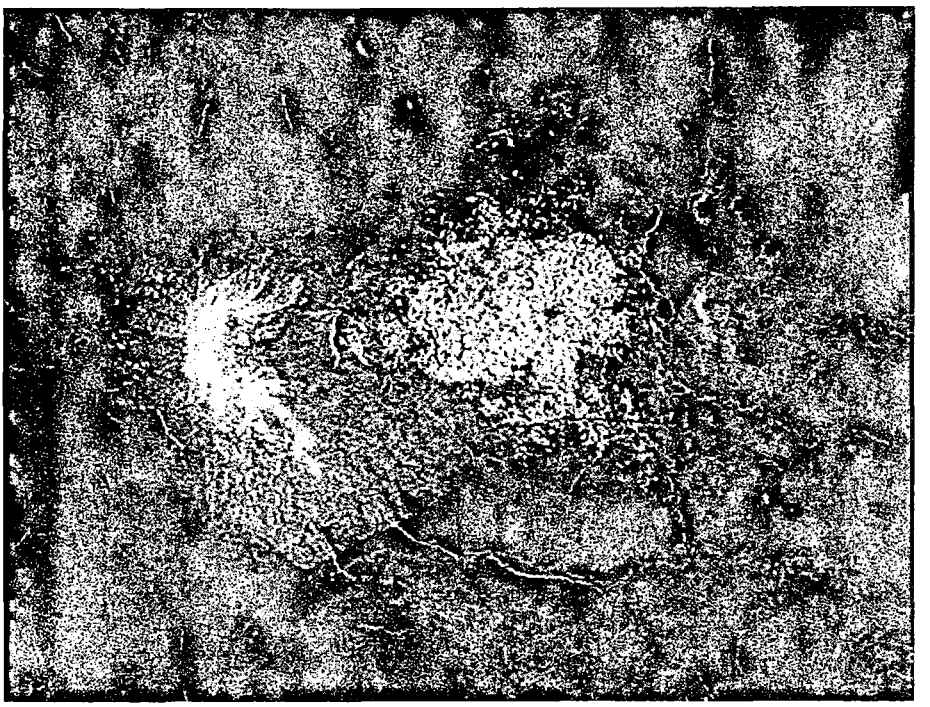

Fig. 15. An example of a dome (md21), sub-category MD3 situated in eastern Mokosha Mons (55°N, 266°E). The dome has a diameter of *c.* 20 km. The apron to the east has the characteristics of deposits in group one (G1). The proximal zone of the apron is situated on the lower slopes of the dome. The deposits are superimposed on the surrounding fractured plains. Magellan image C1 MIDR 60N097;1. Radar illumination is from the left.

or the top of the dome slope. For detached debris aprons, a minimum area measurement was made which included only the material visible in the SAR images. Debris apron areas range from 11.1 km^2 to 2138.8 km^2, with a mean of 349.5 km^2. The most common range in areas is <100 km^2 (Fig. 25). Within the different groups, deposits in group one cover areas ranging from *c.* 150 km^2 to *c.* 2150 km^2 with a mean of *c.* 800 km^2 (Table 2). Deposits in group two have similar characteristics ranging from *c.* 150 km^2 to 1450 km^2 with a mean of *c.* 600 km^2. The areas covered by deposits in group three are smaller than those in the previous groups ranging from *c.* 10 km^2 to *c.* 200 km^2. The areas of deposits in group four range between *c.* 10 km^2 and *c.* 300 km^2 with a mean of *c.* 70 km^2.

Attempts to measure the volume of deposits were restricted by the resolution of the data. It was not possible to determine whether a debris mass had been modified by secondary processes, or what the pre-event topography had been. The absence of headscarps in many instances also hindered attempts to approximate pre-event dome slopes. Crude estimates of the volume of a deposit (assuming a uniform thickness), were possible using the product of the debris apron area and marginal thickness. However, thickness estimates were only possible on debris masses that contained large hummocks, and were dependent upon the orientation of the deposits relative to the SAR look direction and incidence angle. Due to the limited number of volume estimates obtained, deposits are compared by their respective areas, rather than by volume.

The fall height of the majority of mass movements could not be determined from the data. Therefore the total vertical distance from the top of a dome to the base was used as a substitute in calculations of the ratio of height to length (H/L). The H/L ratio gave the angle of a line connecting the uppermost point of a dome with the toe of a deposit. The calculation of H/L is based on the equation used by Heim (1932), which used the uppermost point of a headscarp and the lowest point along the toe of a deposit. The H/L ratio was used to compare the travel

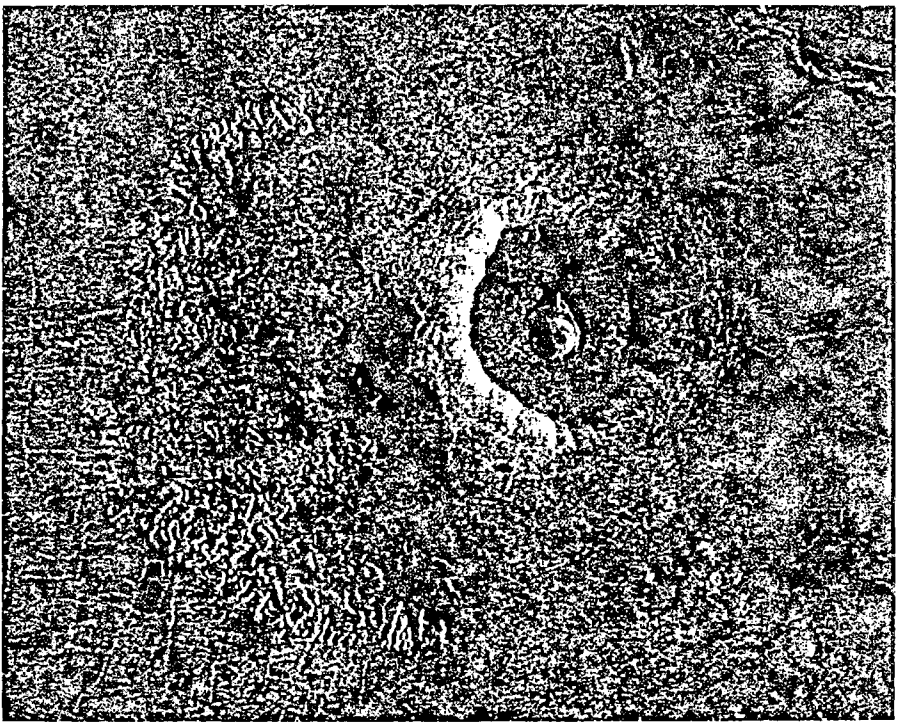

Fig. 16. The dome (md101), sub-category MD3 is situated in Guinevere Planitia (14°N, 299°E). The mass movement to the west has the morphological characteristics of group one (G1). The detached debris apron has a very rough surface texture and fan-shaped plan-form. No large backscar exists that may have been the source of the deposits. The dome is surrounded by circumferential fractures and the deposits appear to mantle the fractured plains. Several east to west trending fractures cross-cut the dome and the deposits. Magellan image C1 MIDR 15N300;1. Radar illumination is from the left.

distance of debris aprons when it was not possible to determine an average coefficient of friction. Shaller (1991) expressed caution in using the H/L ratio to compare the travel distances of large landslides since the value of the ratio coincides with the true coefficient of friction only for those mass movement deposits whose centres of gravity lie close to the toe. However, the calculations of the height to length ratio remain a convenient approximation of true friction for comparing the behaviour of large debris masses since it underestimates the friction coefficient. The H/L ratios for debris aprons on Venus ranges from 0.001 to 0.4 with a mean of 0.06 (Table 2). The deposits in group one have a range in H/L values between 0.001 and 0.01 with a mean of 0.02. The ratios for the other groups of deposits are higher ranging between 0.04 and 0.1 with a mean of 0.08 for group two, between 0.04 and 0.1 with a mean of 0.04 for group three, and between 0.02 and 0.4 with a mean of 0.13 for deposits in group four.

Destructive geomorphic processes modifying domes

Destructive geomorphic processes on volcanic domes on Earth can occur during or after emplacement, exhibiting a broad range of complexity, diversity and magnitude. During dome emplacement slope failure of the edifice margin under gravity may occur as a result of oversteepening (Neumann van Padang 1933; van Bemmelen 1949; Francis *et al.* 1974; Ui 1983; Siebert 1984), and this in turn can lead to decompression of the magma which will cause an explosion (Fink & Kieffer 1993; Gorshkov 1959; Voight *et al.* 1981; Fisher *et al.* 1987). Such an explosion can result in pyroclastic flows and surges (Walker & McBroome 1983; Cas & Wright 1987; Sato *et al.* 1992; Nakada & Fujii 1993). After an eruption has ceased, further destructive processes are mainly the result of gravitationally induced slope failure, for example caused by seismic activity. These geomorphic

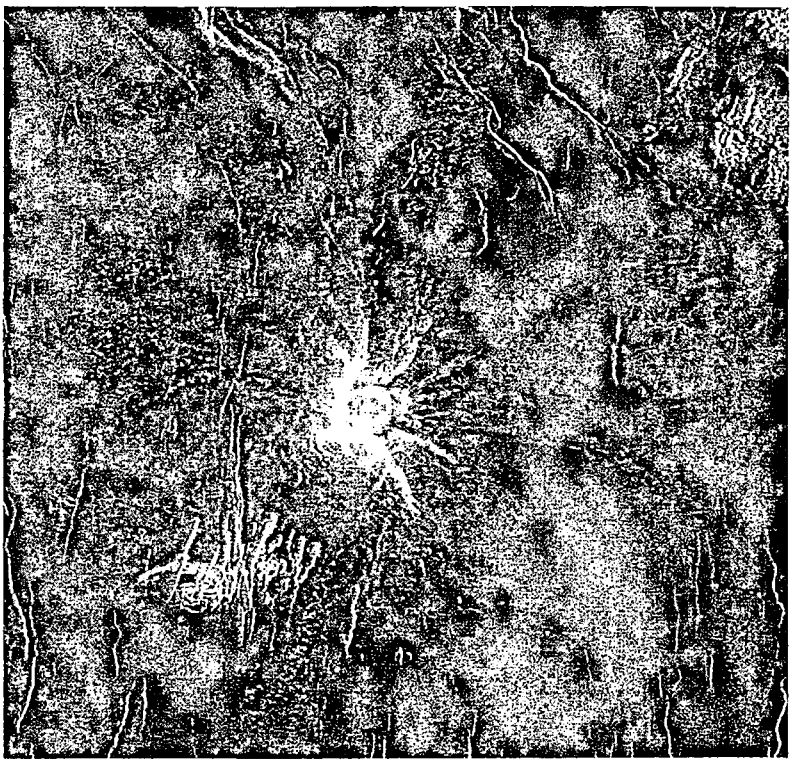

Fig. 17. The dome (md210), sub-category MD3 is situated in Navka Planitia (260°S, 296.7°E). The dome has a diameter of *c.* 15 km and a calculated height of 2.5 km. The mass movements have the characteristics of group two (G2). The detached debris aprons have long, narrow and irregular plan-forms that spread towards the distal margins. The deposits are cross-cut by north to south trending fractures and grabens. Magellan image C1 MIDR 30S297;1. Radar illumination is from the left.

processes, which can be divided into either explosive or non-explosive events, are now examined to determine which could have operated on domes on Venus.

The high atmospheric pressures on Venus (95 bar at 6051.8 km mpr), will inhibit the expansion of exsolved bubbles in magmas and consequently the stress in bubble walls, and in turn, the energy available to drive an eruption. The reduced atmospheric pressure at the summit of large volcanoes will allow for greater expansion of exsolved bubbles in magmas rising in conduits. Explosive activity will be limited to cases in which large bubbles are produced by coalescence, or where the magma initially had a high volatile content. Pyroclastic eruptions involving continuous magma disruption by gas bubble growth can only occur if the exsolved magma volatile contents exceed several weight per cent. Calculated minimum volatile contents on Venus required to cause disruption are high compared with Earth; for CO_2, a value of 5% is required in the lowlands, and 2% in the highlands (Head & Wilson 1986). The high atmospheric pressures and temperatures will also suppress the rise of a convective plume and consequently limit the area of dispersal of entrained material. The development of a high convecting plume requires an unlikely combination of high volatile contents, high initial temperatures, and high altitude eruptions (Thornhill 1993). If pyroclastic events do occur on Venus, explosively ejected material is likely to have low fragment velocities and undergo rapid clast cooling by convective heat loss. Ground-hugging pyroclastic flows are therefore the most likely product of explosive eruptions on Venus. Debris deposits in group three (G3) that are composed of relatively uniformly sized smooth material could be derived from explosive activity, which may explain why the upper surfaces of the two domes on the summit of

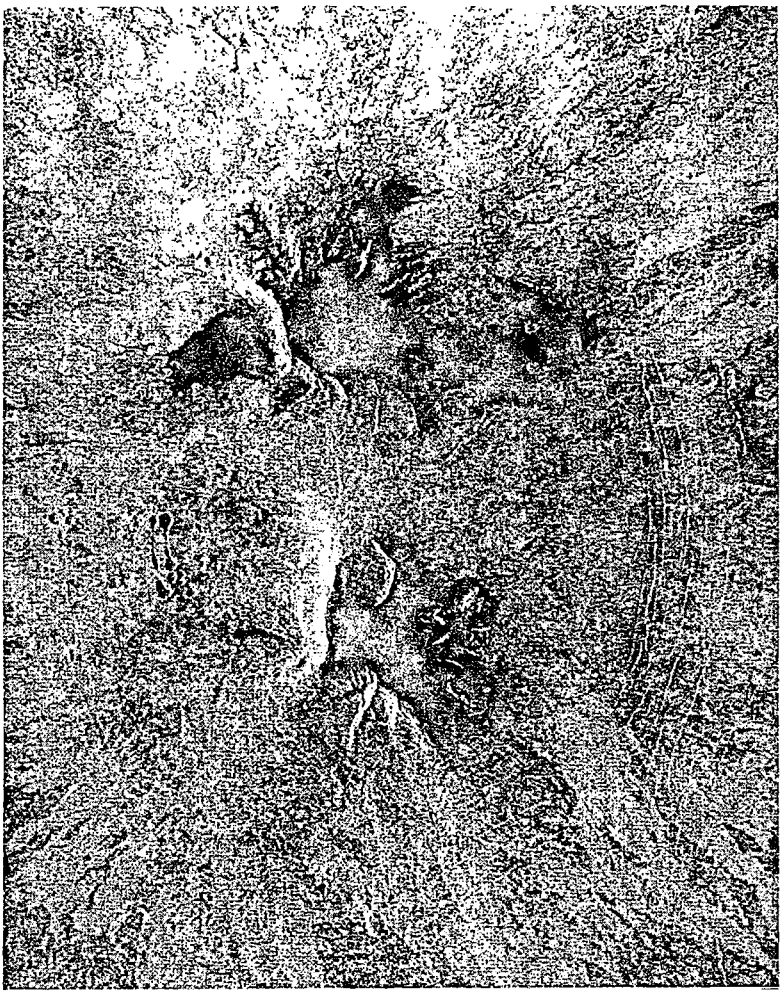

Fig. 18. Two domes (md122, md126), sub-category MD3, situated on the summit of the shield volcano Sapas Mons (8.5°N, 188.2°E). The northern dome is *c.* 20 km in diameter. Both domes have deposits with the characteristics of group three (G3), have long, narrow and irregular plan-forms. The debris travelled down narrow canyons and spread out once away from the base of the dome. The deposits are superimposed on the surrounding lava flows. C1 MIDR 15N188;1. Radar illumination is from the left.

Sapas Mons (8.8°N, 188.2°E) are mantled in radar-dark, smooth material ranging in size from 5 mm to 20 mm (Fig. 18). The domes occur at an elevation of 6054.3 km mpr where volatile exsolution would be easier than on the plains. The morphology of the deposits indicates that localized events occurred and that flows travelled down valleys and spread out over plains forming flat or sub-horizontal upper surfaces. They could have formed from block-and-ash flows or from scoria-flow deposits triggered by the collapse of blocks on the dome margins. These events would have required only localized volatile concentrations, making them far more likely than a large explosive eruption. The existence of small pit craters on many domes on Venus, which may have resulted from small explosive events, suggests that localized volatile concentrations have occurred in some domes.

Non-explosive mass movement can result from gravitational collapse of the front of a lava dome. In this case, initial velocities are determined solely by the conversion of potential energy into kinetic energy as fragments fall. All slope-forming materials have a tendency to

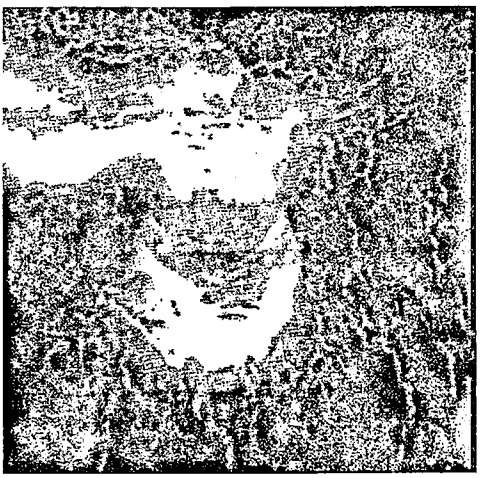

Fig. 19. A dome (md65), sub-category MD3, situated in Niobe Planitia (27.5°N, 134.8°E). The dome is *c.* 20 km in diameter. The debris deposit to the northwest has the characteristics of group four. It is 8.8 km wide and extends 15.2 km. The deposits mantle the fractured plains which surround the dome. C1 MIDR 30N135;1. Radar illumination is from the left.

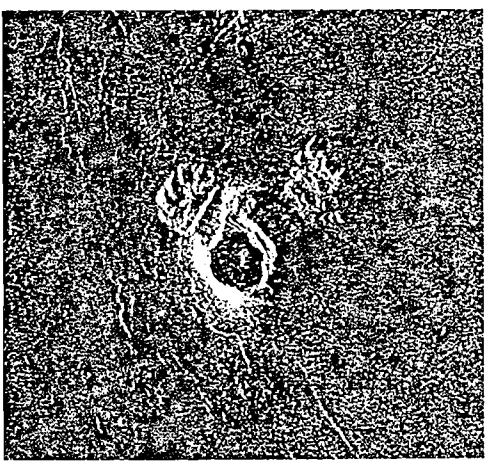

Fig. 20. The dome (md206), sub-category MD1, is situated in Navka Planitia (25.4°S, 308°E). The dome is *c.* 10 km in diameter. The debris aprons to the northwest and northeast have the characteristics of group four (G4). The deposit to the northeast has a rough surface texture and irregular plan-form. The deposit to the northwest has a steep backscarp and a lobate plan-form. The debris aprons are superimposed on the surrounding plains. Magellan image C1 MIDR 30S315;1. Radar illumination is from the left.

move downwards under the influence of gravity, which is counteracted by a shearing resis-tance. For a given slope, if stress exceeds resistance then failure occurs and the slope will move to a new position of equilibrium (Brunsden 1979). Slope failures can be triggered either by internal changes of shearing resistance or by external factors that produce an increase in shear stress. No change in the shearing resistance of the

Fig. 21. The dome (md176), sub-category MD2 is situated to the south of Atla Regio (16.2°S, 211.7°E). The dome is *c.* 25 km in diameter and 2.8 km high. The deposits on the southern part of the dome have the characteristics of group four (G4). The surface textures of the deposits are rough and the plan-forms blunt. Several arcuate backscarps have deposits at their base. The deposits are superimposed on east–west trending fractures. Magellan image C1 MIDR 15S215;1. Radar illumination is from the left.

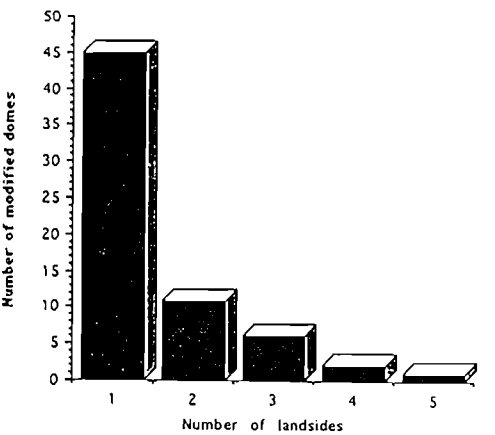

Fig. 22. Histogram showing the number of debris aprons per dome. Population 105.

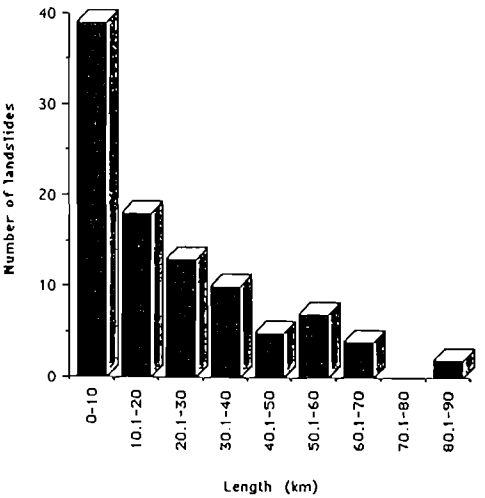

Fig. 23. A plot of the frequency of mass movement travel distances. Population 105.

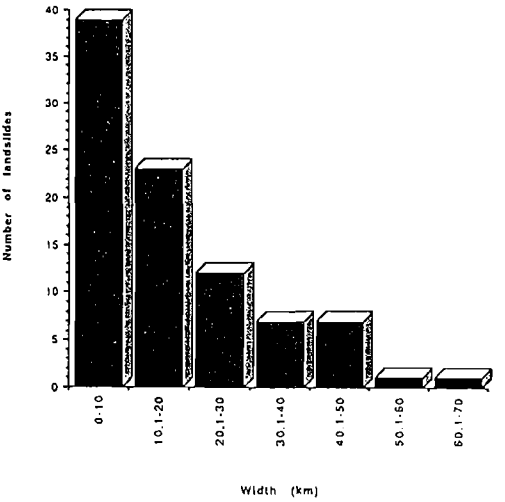

Fig. 24. Histogram showing the width of debris deposits associated with domes. Population 105.

slope-forming materials is necessary for failure to occur (Terzaghi 1960).

Internal causes of slope failure during emplacement of domes (Williams 1932; Swanson *et al.* 1987; Beget & Kienle 1992; Nakada & Fujii 1993) arise from overloading of a slope by lavas, excess weight of lavas at the top of a slope, and from rapid emplacement leading to oversteepening of a flow front (Siebert 1984; Guest *et al.* 1984). On Venus, as on Earth, the eruption style, rate, rheology and local topography are likely to have determined the internal stresses experienced during the growth of domes. Failure of a dome as a result of overloading of a slope by lavas, will depend on the mode of emplacement. If a dome's growth is endogenous and a crust forms on the margin, then lateral advance can occur only as a result of stresses imposed by newer lavas. If the stress exceeds the strength of the crust, then slope failure will occur and the flow front advances. If a dome is exogenous then new lavas erupting onto the surface of the dome can cause slope failure due to the weight of lavas exceeding the strength of the slope.

The morphology of venusian domes suggests that growth was endogenous. On terrestrial domes (e.g. Lassen Peak, California; Mount Pelée, Martinique; Metcalf dome, Alaska (MacDonald 1972)), talus occurs around the margins. Many domes on Venus have radar-bright margins that may be interpreted as rough talus. On terrestrial domes, talus results from fracturing of the crust as the dome grows, and the stresses set up in the rock as it contracts during cooling. The resulting angular blocks are moved by the growing dome and those on the margin topple down to the base. Three monolithological landslides have occurred in the

Table 2. *Morphometric characteristics of the different groups (G1–G4) of debris aprons associated with modified domes*

Group	Area (km^2)	Length (km)	Width (km)	Height (km)	*H/L*	Total
Ranges						
G1	148–2138.8	21.8–80.7	4.2–62.5	0.2–1.4	0.001–0.01	32
G2	171.1–1459.7	14.4–68.8	6.8–26.1	2.2–2.8	0.04–0.1	11
G3	9–202.5	10.7–21.8	2.1–12.8	0.9–1.2	0.04–0.1	7
G4	11.1–315.6	2–18.7	0.5–26.7	2.8–0.2	0.02–0.4	54
Means						
G1	805.4	41.5	31.6	0.6	0.02	32
G2	626.7	44.1	14.6	2.5	0.08	11
G3	62.6	15.9	3.2	0.7	0.04	54
G4	77.8	8.04	9.5	1.3	0.13	54

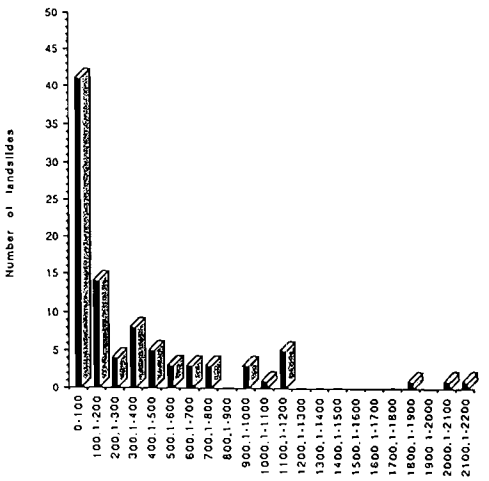

Fig. 25. Graph showing the areas covered by debris aprons associated with domes. Population 105.

Chaos Crags region of Lassen Peak, California. These were formed at different periods during the growth of the same dacite dome as a result of construction of gravitationally unstable jointed rock masses (Eppler *et al.* 1987). Progressive failure of jointed rock slopes occurs along joints and other discontinuities, along which strength is a product of friction between the rock faces (Terzaghi 1960, 1962). The total effective cohesion or resistance of jointed rock slopes is equal to the combined strength of blocks plus the friction between the joint planes. If stress increases slowly, fracturing occurs progressively, resulting in stress increasingly being concentrated on the remaining intact rock. Once the reduction in strength reaches a point where the average shear resistance is equal to the average shear stress, the slope will fail to a stable angle which is dependent on the jointing pattern and the orientation of the discontinuities relative to the slope.

An external cause of mass movement on volcanic edifices on Earth is seismicity. This can produce structural alteration of the constituent parts of a slope (by disturbing intergranular bonds, and by decreasing cohesion and internal friction), dislodgement of otherwise stable slopes, and horizontal and vertical fault movements resulting in increased slope angles. Other external causes of slope failure include weathering and erosion. In the absence of any meaningful seismic data for Venus, the existence of seismic events is inferred from the evidence of extensive faulting and deformation seen in the images. Slope failure triggered by seismicity appears possible, given the existence of large fractures around many domes and the interrelationship between many domes and circumferential fractures. A strong association has also been recognized on Earth between seismicity and the sub-surface movements of magma. Studies of earthquake-triggered slope failures (Keefer 1984; Wilson & Keefer 1985; Cotecchia 1989; Crozier 1991; Perrin & Hancox 1992) have shown that rockfalls and rockslides are some of the most abundant types of failure. Seismic events are inferred to have triggered slope failures on volcanic edifices at Socompa, Chile (Francis & Self 1987), on the flanks of Mauna Loa, Hawaii (Lipman *et al.* 1988), and on Vesuvius, Italy (Hazlett *et al.* 1991). It therefore seems reasonable to suggest that some slope failures on Venus may have been seismically triggered.

Categories of debris deposits that show no evidence of having been triggered by explosive events include deposits in groups one (G1), two (G2) and four (G4). The characteristics of the debris deposits in groups one (G1) and two (G2) are morphologically similar to terrestrial volcanic debris avalanche deposits. In plan view, the deposits in these two groups often have long travel distances relative to widths, and are fan-shaped with lobate or irregular lateral and distal margins (Fig. 26). Terrestrial debris avalanche deposits result from the downward movement of newly detached fragments of bedrock moving on bedding, joint or fault surfaces or any other plane or separation (Sharpe 1938). The failure of a rockmass is followed by rapid and extensive movements of debris as slide blocks disintegrate and move away from the source. Debris avalanche deposits consist of a poorly sorted mixture of brecciated debris, the dominant constituent being lithic material of the source volcano, and are generally more poorly sorted than pyroclastic flow deposits, and typically have coarser textures. Hummocky surfaces have been noted as typical topographic features of volcanic debris avalanche deposits (Siebert 1984; Ui 1983). Each hummock consists of one or a few megablocks composed of a former portion of the volcanic edifice transported by the avalanche. Hummocks may have been formed by horst and graben formation during lateral spreading (Voight *et al.* 1981; Glicken *et al.* 1981). Hummocky surfaces, characteristic of deposits in groups one and two, are similar to those in the Pungarehu formation at Egmont, New Zealand (Neall 1979). If the surfaces of venusian domes are composed of angular blocks, they will be susceptible to failure along planes of weakness especially where blocks dip

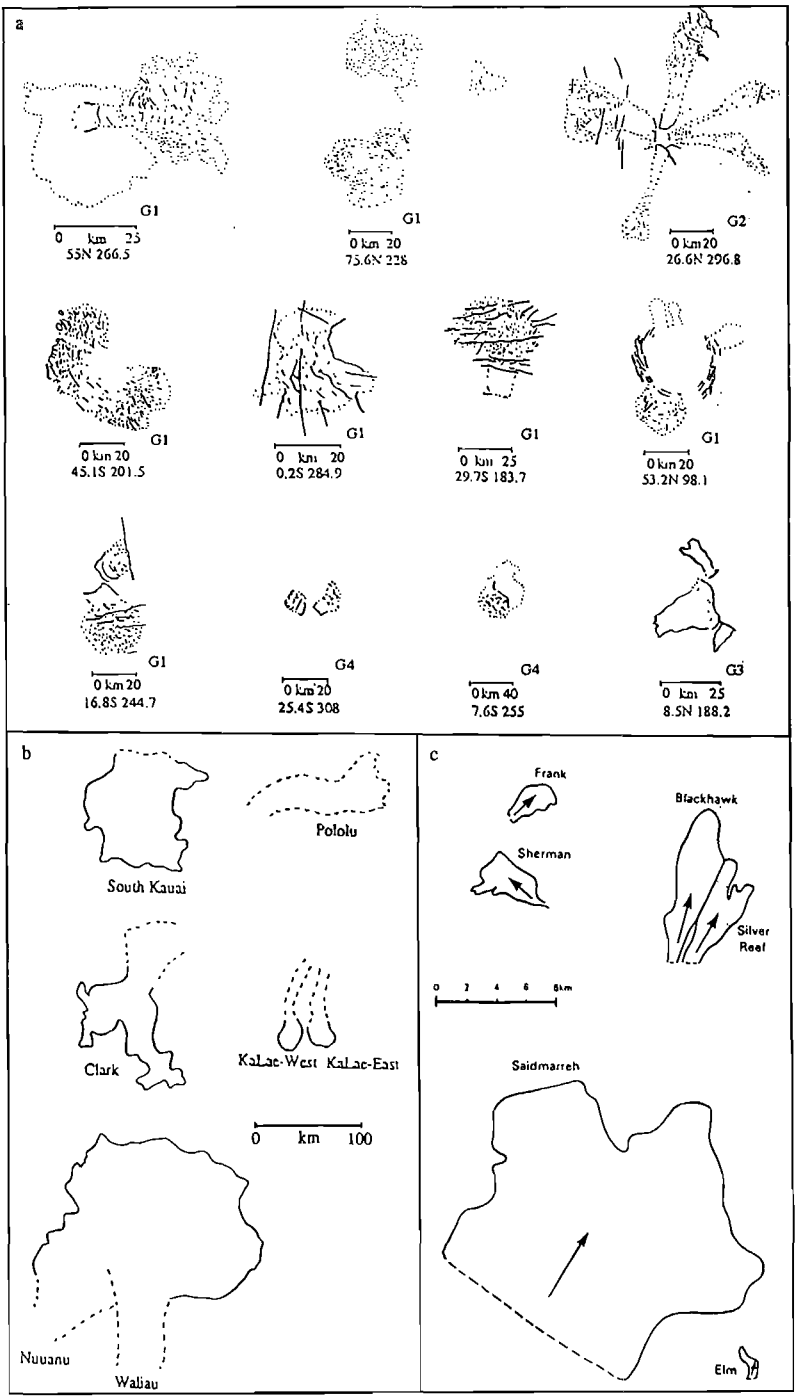

Fig. 26. Schematic diagram showing the plan-forms of debris aprons; (a) shows debris aprons associated with domes on Venus, (b) and (c) show sub-marine (adapted from Moore *et al.* 1989) and sub-aerial (adapted from Shreve 1968) debris aprons on Earth.

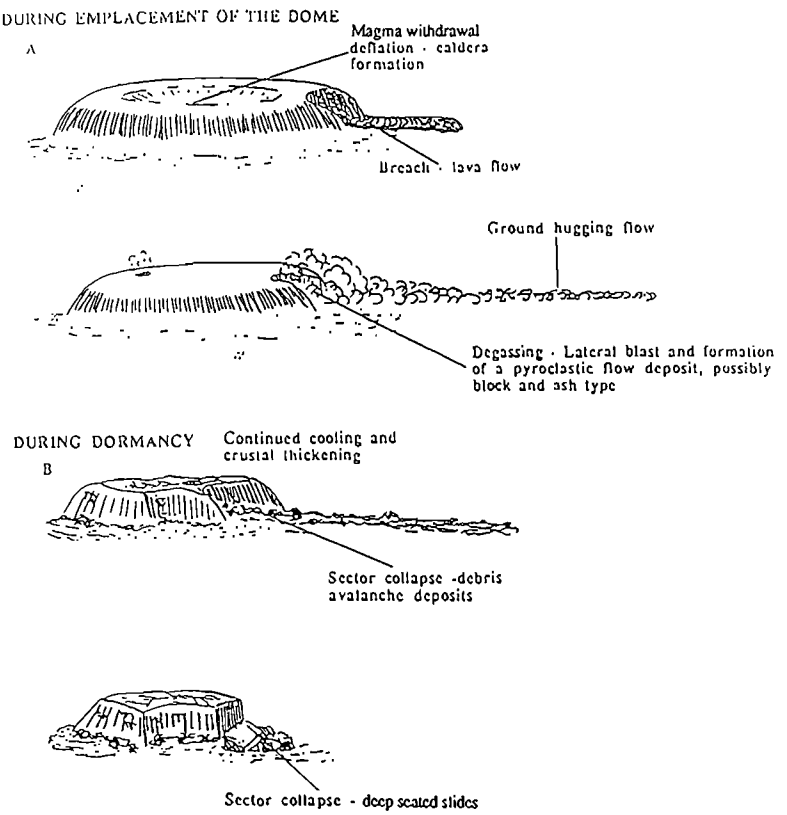

Fig. 27. Schematic representation of destructive processes responsible for the modification of domes during emplacement and after dormancy: (A) shows the upper surface domes being modifed by magma withdrawal, caldera formation or deflation. During dome growth oversteepening of the margins may result in a breach. Mass movements producing deposits with the characteristics of G3 may be caused by explosions; (B) shows modification of domes by slope failure after the dome has ceased to grow. Slope failures on the margins of rigid domes may result in deposits with the characteristics of G1, G2 and G4.

at angles close to the angles of friction on those surfaces. Large rock masses that have failed may disintegrate as they move away from the dome forming brecciated debris.

Some of the deposits in groups one and two are also similar to terrestrial non-volcanic landslides, such as Blackhawk and Silver Reef, California (Shreve 1968), Loma Redonda, Loma de la Aspereza, Avalancha del Zarzo 1 and Avalancha del Zarzo 2, Argentina (Foque & Strecker 1988), as well as seven landslides on Mars (Shaller 1991). In plan, the Blackhawk landslide forms a narrow, symmetrical lobe that is distally raised (Fig. 26). The deposit has an overall length of 8 km and an average width of 2.4 km. The depth of the deposit increases uniformly from the proximal to distal zone and the surface of the slide consists of low, rounded hills and small, closed basins. Several large volcanic sub-marine deposits off the Hawaiian coast also have similar morphological characteristics to venusian deposits in groups one and two (Fig. 26). These have well-developed backscarps, and large blocks in their mid-sections that terminate in aprons of hummocky terrain (Lipman *et al.* 1988; Moore *et al.* 1989).

The characteristics of the deposits in group four are similar to non-explosively triggered deep-seated slides on Earth. These slides typically occur along lines of weakness such as joints, faults or possible bedding planes. Slides that include a planar element exhibit severe distortions and fracturing of the mass. Those slides that occur on curved failure surfaces have been termed 'rotational' slides and can be single, multiple or successive (Hutchinson 1968). The main part of the failure surface is controlled by shear and tension cracks that often form in the upper parts of the slope during the initial phases of movement. These cracks close as the mass

back-tilts during rotation. Several domes such as those in Niobe Planitia (27.5°N, 134.8°E), and in Navka Planitia (25.4°S, 308°E), have slope morphologies characteristic of having formed as a result of a single rotational slide. Multiple rotational slides occur as a retrogressive series of slips, each on a curved surface that is linked tangentially to a common failure line (Brunsden 1979). In plan-form such deposits often show a sequence of arcuate blocks arranged one behind another. The complex of scarps on the dome south of Atla Regio (16.2°S, 211.7°E) has the characteristics of having formed from multiple rotational slides.

It appears from analysis of the image data, that destructive processes that modify domes can be divided into those that are accompanied by an explosive component, and those that are non-explosive. Given the constraints imposed on explosive activity by atmospheric conditions, and the high magma volatile concentrations needed to cause disruption, the most likely internal causes of slope failure on venusian domes are the result of localized volatile accumulations and the oversteepening of slopes during dome growth (Fig. 27). The formation of a chilled carapace composed of angular blocks during the growth of venusian domes, will produce slopes predisposed to progressive failure along joints and other discontinuities. The internal stresses within a growing dome, combined with external factors such as the nature of the local topography will control the magnitude and frequency of slope failures. The majority of slope failures appear to have occurred after domes had cooled, and were solid. Some large slope failures were probably seismically triggered. The characteristics of deposits suggest that different forms of mass movement have occurred. The deposits in G1 and G2 have characteristics similar to those of terrestrial volcanic debris avalanche deposits, while those in G3 are similar to terrestrial pyroclastic flow deposits. The characteristics of G4 are analogous to deep-seated slides on Earth.

Conclusion

A range of modified dome morphologies occurs on Venus. The majority of domes on Venus are an order of magnitude larger in diameter than sub-aerial domes on Earth. Five sub-categories of modified domes can be recognized that have the common characteristic of scalloped margins. Domes are more common on Venus than has previously been proposed. Mass movement deposits associated with domes on Venus can be divided into four distinct morphologies. Each morphological group possesses unique surface textures and plan-forms, and has distinctive morphometric characteristics. The deposits in groups one and two have average travel distances greater than 40 km and the lowest coefficients of friction of the four groups, while deposits in group four have the smallest average travel distances and highest coefficients of friction.

Slope failures on venusian domes appear to have been triggered by explosive and non-explosive events. The conditions on Venus will inhibit the sub-surface exsolution of volatiles, so for pyroclastic events to occur, magma volatile contents must exceed 5% in the lowlands. Unless the volatile content and initial eruption temperatures are high, then the formation of a convective plume will be unlikely and the dense atmosphere will favour the production of ground-hugging flows. Domes with large downsags indicate that volatiles were released through non-explosive degassing, though small pit craters are likely to have formed by explosion resulting from localized volatile concentrations. The smooth surface textures and confined plan-forms of deposits in group three are similar to terrestrial pyroclastic flows. These are thought to have occurred during the emplacement of a dome from the collapse of blocks on the dome margins, or through localized volatile enhancement building stresses greater than the tensile strength of the local rock resulting in an explosively directed blast. The surface textures and plan-forms of the deposits in groups one and two are similar to volcanic debris avalanche deposits on Earth. These have long travel distances, low coefficients of friction and cover large areas. The characteristics of the fourth group of deposits are similar to those resulting from deep-seated slides on Earth. The largest of these removed substantial volumes of material. The blocky nature of deposits indicates that those in groups one, two and four were emplaced after the dome had cooled following the cessation of an eruption. Slope failures are likely to have occurred along structural discontinuities. The characteristics of domes and their associated deposits suggest they are composed of a relatively homogeneous rock.

References

BEGET, J. E., & KIENLE, J. 1992. Cyclic formation of debris avalanches at Mount St Augustine volcano. *Nature*, **356**, 701–704

BRUNSDEN, D. 1979. Mass movements. *In*: EMBLETON, C. & THORNES, J. B. (eds) *Process in Geomorphology*. Arnold, London.

BULMER, M. H. 1994. *An examination of small volcanoes in the plains of Venus; with particular reference to the evolution of domes.* PhD Thesis, University of London, Senate House, England.

——, ——, BERATAN, K., MICHAELS, G. & SAUNDERS, S. 1992*a*. Debris avalanches and slumps on the margins of volcanic domes on Venus: characteristics of deposits (abstract). *International Colloquium on Venus.* Lunar & Planetary Institute Contribution, **789**, 14–15.

——, ——, MICHAELS, G. & SAUNDERS, S. 1993. Scalloped margins domes: What are the processes responsible and how do they operate? (abstract). *Lunar and Planetary Science*, **24**, 215–216.

——, —— & STOFAN, E. R. 1992*b*. Calderas on Venus (abstract). *Lunar Planetary Science*, **23**, Part 1, 177–178.

CAS, R. A. F. & WRIGHT, J. V. 1987. *Volcanic Successions.* Allen and Unwin, Winchester, Mass.

COTECCHIA, V. 1989. Earthquake-prone environments. *In*: ANDERSON, M. G. & RICHARDS, K. S. (eds) *Slope stability.* Geotechnical Engineering and Geomorphology, J. Wiley & Sons, Chichester, 287–330.

CROZIER, M. J. 1991. Determinatin of palaeoseismicity from landslides. *In*: BELL (ed.) *Landslides.* Balkema, Rotterdam.

EPPLER, D. B., FINK, J. & FLETCHER, R. 1987. Rheologic properties and kinematics of emplacement of the Chaos Jumbles rockfall avalanche, Lassen volcanic National Park, California. *Journal of Geophysical Research*, **92**(B5), 3623–3633.

FINK, J. H. & KIEFFER, S. W. 1993. Estimate of pyroclastic flow velocities resulting from explosive decompression of lava domes. *Nature*, **363**, 612–615.

FISHER, R. V., GLICKEN, H. X. & HOBLITT, R. P. 1987. May 18, 1980. Mount St. Helens deposits in South Coldwater Creek, Washington. *Journal of Geophysical Research*, **92**, 10 267–10 283.

FOQUE, L. & STRECKER, M. R. 1988. Large rock avalanche deposits (Sturzstrome, sturzstroms) at Sierra Aconquija, northern Sierras Pameanas, Argentina. *Eclogae Geolicae Helvetiquw*, **81**(3), 579–592.

FRANCIS, P. W. & SELF, S. 1987. Collapsing volcanoes. *Scientific American*, **256**, 90–97.

——, ROOBOL, M. J., WALKER, G. P. L., COBOLD, P. R. & COWARD, M. P. 1974. The San Pedro and San Pablo volcanoes of North Chile and their hot avalanche deposits. *Geologische Rundschau*, **63**, 357–388.

GLICKEN, H., VOIGHT, B. & JANDA, R. J. 1981. Rock-slide debris avalanche of May 18, 1980, Mount St. Helens volcano (abstract). *IAVCEI Symposium on Arc Volcanism, Tokyo and Hakone*, **22**, 109–110.

GORSHKOV, G. S. 1959. Gigantic eruption of the volcano Bezymianny. *Bulletin of Vulcanology*, **20**, 77–112.

GUEST, J. E., BULMER, M. H., AUBELE, J. *ET AL.* 1992*a*. Small volcanic edifices and volcanism in the plains of Venus. *Journal of Geophysical Research*, **97**(E8), part 2 15 949–15 966.

——, ——, BERATAN, K., MICHAELS, G., DESMARIS, K. & WEITZ, C. 1991. Slope failure of the margins of volcanic domes on Venus (abstract). *EOS Transactions American Geophysical Union*, **72**, 278–279.

——, ——, ——, —— & SAUNDERS, S. 1992*b*. Gravitational collapse of the margins of volcanic domes on Venus (abstract). *Lunar and Planetary Science*, **23**, Part 1, 461–462.

——, CHESTER, D. K. & DUNCAN, A. M. 1984. The Valle Del Bove, Mount Etna: its origin and relation to the stratigraphy and structure of the volcano. *Journal of Volcanology and Geothermal Research*, **21**, 1–23.

HAZLETT, R. W., SCANDONE, R. & BUESCH, D. 1991. Unusual slope failures and related deposits of the 1944 eruption of Mount Vesuvius, Italy. *Journal of Volcanology and Geothermal Research*, **47**, 249–264.

HEAD, J. W. & WILSON, L. 1986. Volcanic processes and landforms on Venus: Theory, predictions, and observations. *Journal of Geophysical Research*, **91**, 9407–9446.

——, CRUMPLER, L. S., AUBLELE, J. C., GUEST, J. E. & SAUNDERS, R. S. 1992. Classification of volcanic features and structures, associations, and global distribution from Magellan data. *Journal of Geophysical Research*, **97**(E8), 13 153–13 198.

HEIM, A. 1932. *Bergsturz und Menschenleben.* Fretz und Wasmuth, Zurich.

HUTCHINSON, J. N. 1968. Mass movement. *In*: FAIRBRIDGE, R. W. (ed.) *Encyclopedia of Earth Sciences.* Reinhold, New York, 688–695.

KEEFER, D. K. 1984. Landslides caused by earthquakes. *Geological Society of America Bulletin*, **95**, 406–421.

LIPMAN, P. W., BANKS, N. G. & RHODES, J. M. 1985. Gas-release induced crystallization of 1984 Mauna Loa magma, Hawaii, and effects on lava rheology. *Nature*, **317**, 604–607.

——, NORMARK, W. R., MOORE, J. G., WILSON, J. & GUTMACHER, C. E. 1988. The giant submarine Alika debris slide, Mauna Loa, Hawaii. *Journal of Geophysical Research*, **93**, 4279–4299.

MACDONALD, G. A. 1972. *Volcanoes.* Prentice-Hall, Englewood Cliffs, New Jersey.

MOORE, J. G., CLAGUE, D. A., HOLCOMB, R. T., LIPMAN, P. W., NORMARK, W. R. & TORRESAN, M. E. 1989. Prodigious submarine landslides on the Hawaiian Ridge. *Journal of Geophysical Research*, **94**, 17 465–17 484.

NAKADA, S. & FUJII, T. 1993. Preliminary report on the activity at Unzen Volcano (Japan), November 1990–November 1991: Dacite lava domes and pyroclastic flows. *Journal of Volcanology and Geothermal Research*, **54**, 319–333.

NEALL, V. E. 1979. *Sheets P19, P20 and P21, New Plymouth, Egmont, and Manaia* (1st edn). Geological map of New Zealand 1 : 500 000, three maps and notes. NZ Dept. Sci. Ind. Res., Wellington.

NEUMANN VAN PADANG, M. 1933. De uitbarsting van den Merapi (Midden Java). *In*: *de jaren 1930–31. Ned. Indes. Dienst Mijnbouwk. Vulkan. Seism. Mededel.*, 12.

PAVRI, B., HEAD, J. W., KLOSE, K. B. & WILSON, L. 1992. Steep sided domes on Venus: Characteristics, geological setting, and eruption conditions from Magellan data. *Journal of Geophysical Research*, **97**(E8), 13 445–13 478.

PERRIN, N. D. & HANCOX, G. T. 1992. Landslide-dammed lakes in New Zealand – preliminary studies on their distribution, causes and effects. *Proceedings of Sixth Internatational Symposium on Landslides, Christchurch*. 1–10.

SATO, H., FUJII, T. & NAKADA, S. 1992. Crumbling of dacite dome lava and generation of pyroclastic flows at Unzen volcano. *Nature*, **360**, 664–666.

SHALLER, P. J. 1991. *Analysis and Implications of Large Martian and Terrestrial Landslides*. PhD Thesis. California Institute of Technology.

SHARPE, C. F. S. 1938. *Landslides and Related Phenomena*. Columbia University Press, New York.

SHREVE, R. L. 1968. *The Blackhawk Landslide*. Geological Society of America, Special Paper, **108**, 47.

SIEBERT, L. 1984. Large volcanic debris avalanches: Characteristics of source areas, deposits, and associated eruptions. *Journal of Volcanology and Geothermal Research*, **22**, 163–197.

SPARKS, R. J. S. 1978. The dynamics of bubble formation and growth in magmas: a review and analysis. *Journal of Volcanology and Geothermal Research*, **3**, 1–37.

SWANSON, D. A., DZURISIN, D., HOLCOMB, R. T. *ET AL.* 1987. Growth of the lava dome at Mount St Helens, Washington. *In*: FINK, J. H. (ed.) *The Emplacement of Silicic Domes and Lava Flows*. Geological Society of America, Special Paper, **212**, 1–16.

TERZAGHI, K. 1960. Mechanism of landslides. *In*: *Application of Geology to Engineering practice*. Berkeley volume, Geological Society of America, 83–123.

——1962. Stability of steep slopes on hard unweathered rock. *Geothechnique*, **12**, 251–270.

THORNHILL, G. D. 1993. Theoretical modelling of eruption plumes on Venus. *Journal of Volcanology and Geothermal Research*, **98**(E5), 9107–9111.

UI, T. 1983. Volcanic dry avalanche deposits – identification and comparison with nonvolcanic debris stream deposits. *Journal of Volcanology and Geothermal Research*, **18**, 135–150.

VAN BEMMELEN, R. W. 1949. *The geology of Indonesia and adjacent archipelago*. The Hague: Government Printing Office.

VOIGHT, B., GLICKEN, H., JANDA, R. J. & DOUGLASS, P. M. 1981. Catastrophic rockslide avalanche on May 18. *In*: LIPMAN, P. W. & MULLINEAUX, D. R. (eds) *The 1980 Eruption of Mount St. Helens, Washington*. US Geological Survey Professional Paper, **1250**, 347–378.

WALKER, G. P. L. & MCBROOME, L. A. 1983. Mount St. Helens 1980 and Mount Pelee 1902 – flow or surge? *Geology*, **11**, 571–574.

WILLIAMS, H. 1932. *The History and Character of Volcanic Domes*. University of California Berkeley, Bulletin of the Department of Geological Science, **21**.

WILSON, R. C. & KEEFER, D. K. 1985. Predicting areal limits of earthquake-induced landsliding. *In*: ZIONY, J. I. (ed.) *Evaluating Earthquake Hazards in the Los Angeles Region – An Earth-Science Perspective*. US Geological Survey Professional Paper, **136**, 317–345.